Journal of
Applied Crystallography

ISSN 0021-8898

Received 16 August 2006
Accepted 24 January 2007

A focusing-geometry small-angle neutron scattering instrument with a magnetic neutron lens

Takayuki Oku,[a]* Hiroki Iwase,[a] Takenao Shinohara,[a] Satoru Yamada,[a] Katsuya Hirota,[b] Satoshi Koizumi,[a] Jun-ichi Suzuki,[a] Takeji Hashimoto[a] and Hirohiko M. Shimizu[b,c]

[a]JAEA, Tokai, Ibaraki 319-1195, Japan, [b]RIKEN, Wako, Saitama 351-0198, Japan, and [c]KEK, Tsukuba, Ibaraki 305-0801, Japan. Correspondence e-mail: oku.takayuki@jaea.go.jp

We have constructed a focusing-geometry small-angle neutron scattering (FSANS) instrument, SANS-J-II, with two kinds of neutron focusing device: a series of compound refractive lenses made of MgF_2 and a magnetic neutron lens based on an extended Halbach-type sextupole magnet. In this study, we investigated the performance of the FSANS instrument with the magnetic neutron lens. The intensity distribution of a direct neutron beam focused on the detector plane by the magnetic neutron lens had a ratio of the peak height to the background level of $\sim 6 \times 10^4$ for a polarized neutron beam with a polarization degree of ~ 0.99. It is found that a minimum value of the measurable q range [where q is the modulus of the scattering vector and is defined as $q = (4\pi/\lambda)\sin(\theta/2)$, where θ is the scattering angle and λ is the neutron wavelength], $q_{\min}$, of 6.5×10^{-4} Å^{-1} can be achieved by the FSANS instrument with the magnetic neutron lens using neutrons with $\lambda = 6.6$ Å and $\Delta\lambda/\lambda = 0.13$ for the full width at half maximum.

1. Introduction

The measuring efficiency and/or angular resolution of small-angle neutron scattering (SANS) experiments can be improved by focusing neutrons on a detector plane (Alefeld *et al.*, 1997; Choi *et al.*, 2000). Thus, two kinds of neutron focusing lenses (compound refractive lenses and a magnetic focusing lens) have been installed at the SANS instrument SANS-J-II of JRR-3 at the Japan Atomic Energy Agency for focusing-geometry SANS (FSANS) experiments (Koizumi *et al.*, 2006). The compound refractive lenses are biconcave lenses made of MgF_2 (Eskildsen *et al.*, 1998; Choi *et al.*, 2000). The magnetic neutron lens is a sextupole magnet which is considered to be a suitable neutron focusing device for FSANS experiments with polarized neutrons, since the polarized neutrons can be focused by the magnetic neutron lens free from neutron absorption and scattering by substances (Oku *et al.*, 2004, 2005). Depending on the experimental conditions, the appropriate kind of focusing setup can be chosen. In this study, we investigated the performance of the neutron focusing setup using the magnetic neutron lens of SANS-J-II, and we discuss the ability of the FSANS instrument. The performance of the focusing setup using the compound refractive lenses is reported by S. Koizumi *et al.* together with the system and components of SANS-J-II, such as optical devices, detectors and their driving devices (Koizumi *et al.*, 2007).

2. Magnetic neutron lens

As the magnetic neutron lens, we chose an extended Halbach-type permanent sextupole magnet (Oku *et al.*, 2003) because it is lower in cost and more compact than a superconducting magnet (Suzuki *et al.*, 2003), it is maintenance-free and it has good focusing properties (Oku *et al.*, 2006). Fig. 1 shows a schematic cross section of the extended Halbach-type permanent sextupole magnet installed at SANS-J-II.

The magnet consists of 12 segments of strong permanent NdFeB magnets and six segments of the high saturation magnetization material permendule, $Fe_{49}Co_{49}V_2$. The direction of the magnetization

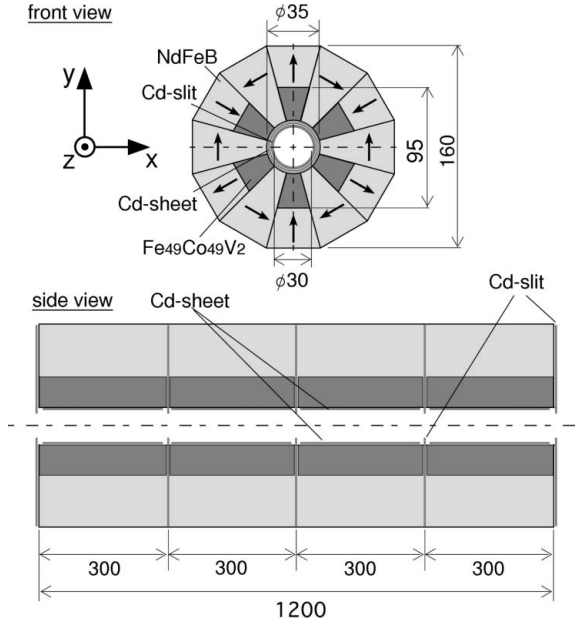

Figure 1
A schematic cross section of the extended Halbach-type permanent sextupole magnet. The arrows show directions of the magnetization. Units: mm.

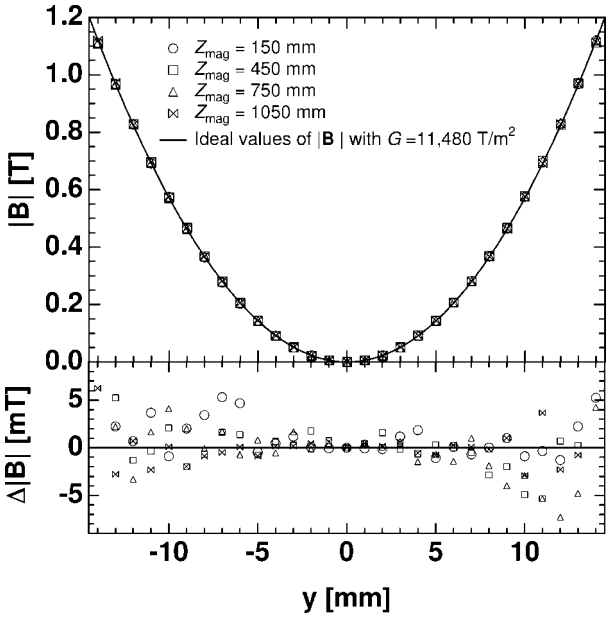

Figure 2
The distribution of the magnetic field strength $|\mathbf{B}|$ inside the magnetic neutron lens. Z_{mag} is the distance from the magnet end along the magnet center axis. $\Delta|\mathbf{B}|$ is the difference between the measured and ideal values of $|\mathbf{B}|$.

vector of each NdFeB segment is assigned as shown in Fig. 1. The permendule compresses and guides the magnetic flux toward the center of the magnet, resulting in an increase of the magnetic field strength inside the magnet by a few tens per cent (Halbach, 1979; Kumada *et al.*, 2001). The inner diameter and length of the magnet are 35 and 1200 mm, respectively. The weight of the magnet is 226 kg including the surrounding Al-alloy frame. The inner surface of the magnet was covered with Cd sheets, and Cd slits with 30 mm-diameter pinholes were set inside the magnet for the suppression of neutron reflection on the inner surface of the magnet as shown in Fig. 1. Therefore, the effective aperture of the magnetic neutron lens is 30 mm in diameter. We performed a magnetic field measurement inside the magnetic neutron lens using a Hall probe. The spatial distribution of the magnetic field strength $|\mathbf{B}|$ inside the magnetic neutron lens is given by $|\mathbf{B}| = (G/2)r_m^2$ with the magnetic field gradient coefficient $G = 11\,480 \pm 281$ T m^{-2}, where r_m is the distance from the magnet center axis (Fig. 2).

3. Experimental setup

The instrumental setup is shown in Fig. 3. The neutron beam was monochromated by using a mechanical velocity selector with a wavelength dispersion $\Delta\lambda/\lambda = 0.13$ for full width at half maximum (FWHM). The magnetic neutron lens has neutron-polarity-dependent focusing properties, *i.e.* it focuses and defocuses neutrons with positive and negative spin polarity, respectively (Shimizu *et al.*, 1998, 1999). Therefore, the neutrons were polarized using FeSi supermirror polarizers. In the setup, two polarizers with different lengths are available; they are referred to as P1 and P2. P1 is designed for high-resolution measurements, has a length of 150 mm and is effective for a incoming neutron beam with a cross section of 1 mm (W) × 1 mm (H). On the other hand, P2, which is designed for high-intensity measurements, is 2500 mm long, has Ni side walls for efficient neutron transfer and has an effective cross section of 20 mm (W) × 50 mm (H) for the incoming neutrons, as depicted in Fig. 4. The polarizer can be chosen depending on the experimental conditions. We use these polarizers in transmission mode so that the output neutron beam from the polarizers has negative spin polarity. Thus, to focus the neutron beam by using the magnetic neutron lens, their spin state must be flipped by π. For this purpose, a two-coil (Drabkin) π flipper (SF) with a triple μ-metal shield (Jones & Williams, 1978) was placed between the polarizers and the magnetic neutron lens (Fig. 3). A guide field for transferring neutrons while conserving their spin states was applied by using solenoid coils (SC1) with their field direction parallel to the neutron beam axis (Fig. 3). The magnetic field distribution deviates from the sextupole field around both ends of the magnetic neutron lens, where nonadiabatic regions are created for neutron spin transportation (Suzuki *et al.*, 2003; Furusaka *et al.*, 1999). To remove the nonadiabatic region by applying a dipole field along the neutron beam axis, solenoid coils (SC2), which generate a field of 1 kGauss at their center position, were set adjacent to the both ends of the magnetic neutron lens (Fig. 3). Then another neutron focusing device, the MgF_2 biconcave compound refractive lenses, which focus the neutrons irrespective of the neutron spin polarity, was also installed at SANS-J-II (Fig. 3) (Koizumi *et al.*, 2007). The intensity distribution of the focused neutron beam was measured by using a photomultiplier-based scintillation two-dimensional detector (PSD) with position resolution of 0.7 mm for the FWHM (Hirota *et al.*, 2005).

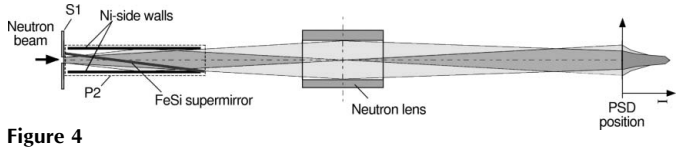

Figure 4
The schematic layout for setups 2 and 3.

4. Experimental results and discussion

As the focal length of the magnetic neutron lens depends on the neutron wavelength λ, we measured the intensity distribution of the neutron beam focused by the magnetic neutron lens as a function of λ. Fig. 5 shows the radial averages of the intensity distributions, where r is the distance from the peak center. The FWHMs of the intensity peaks are plotted in Fig. 6. It was found that the intensity peak became sharpest for λ = 6.6 Å (Fig. 6), suggesting that the focal

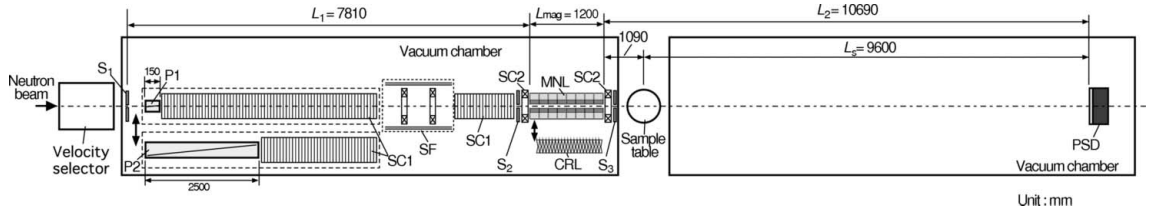

Figure 3
The experimental setup. MNL and CRL are the magnetic neutron lens and the compound refractive lenses, respectively.

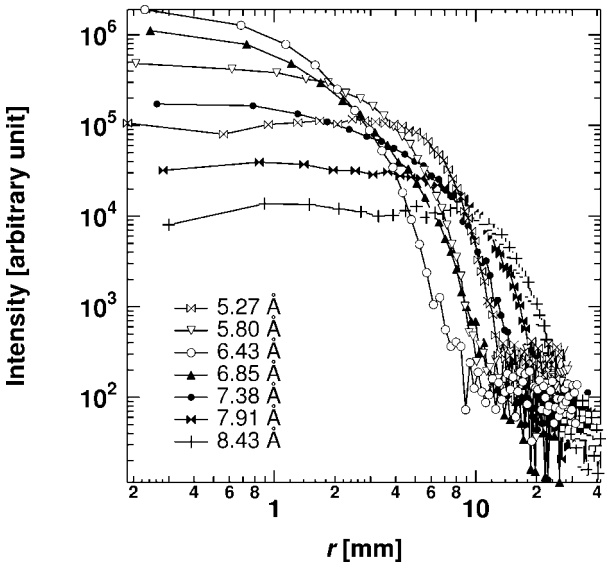

Figure 5
The radial averages of the intensity distribution. r is the distance from the peak center.

condition was satisfied with this wavelength. In the current setup, the focal condition is given by

$$L_{\rm mag} = \alpha\left\{\cot^{-1}\left(\frac{L_1}{\alpha}\right) + \cot^{-1}\left(\frac{L_2}{\alpha}\right)\right\}, \qquad (1)$$

where $\alpha = h/[\lambda(Gm_{\rm n}\mu_{\rm n})^{1/2}]$, $L_{\rm mag}$ is the magnet length, L_1 and L_2 are the flight lengths (Fig. 3), h is Plank's constant, $m_{\rm n}$ is the neutron mass, and $\mu_{\rm n}$ is the neutron magnetic moment (Suzuki *et al.*, 2003). By solving equation (1), we obtained G = 11 580 T m^{-2}, which was consistent with the result of the magnetic field measurement (Fig. 2).

To evaluate the performance of the neutron focusing setup using the magnetic neutron lens of SANS-J-II, we measured the intensity distribution of the neutron beam focused by the collimation setups listed in Table 1, and compared the results.

Here, $\lambda = 6.6$ Å for the focal condition of the magnetic neutron lens. The compound refractive lenses are biconcave-shaped single-crystal MgF_2 lenses whose diameter, curvature radius, and center thickness are 30, 25 and 1 mm, respectively (Koizumi *et al.*, 2007). 70

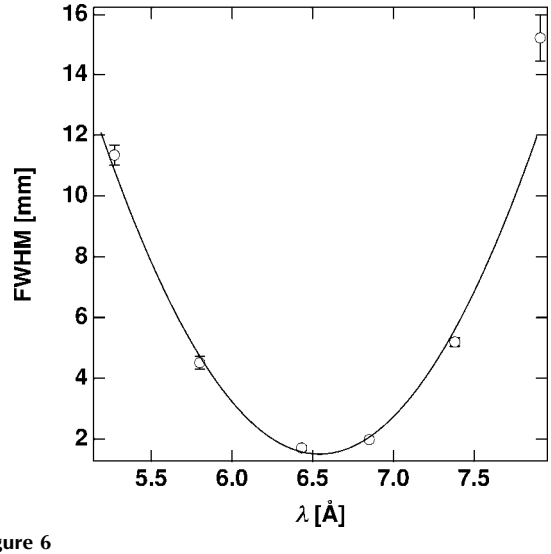

Figure 6
The FWHMs of the intensity peaks as a function of λ.

Table 1
The collimation setups.

Setup	Polarizer	Lens	Size of slit S_1 (mm)	Size of slits S_2 and S_3 (mm)
1	P1	Magnetic neutron lens	1.0 × 1.0	20 × 20
2	P2	Magnetic neutron lens	1.5 × 1.5	20 × 20
3	P2	Compound refractive lens	1.5 × 1.5	20 × 20
4	No polarizer	Compound refractive lens	1.5 × 1.5	20 × 20

pieces of the compound refractive lenses were arranged so as to have nearly the same focal condition as the magnetic neutron lens.

Figs. 7(a) and (b) show the radial distributions of the averaged intensities normalized by the measuring time and the peak intensities, respectively. On the basis of the comparison of the peak intensity normalized by the measuring time (Fig. 7a), it was found that (1) the difference in peak intensity between setups 1 and 2 was explained by the difference of the size of the slit S_1 (Fig. 3), (2) the neutron

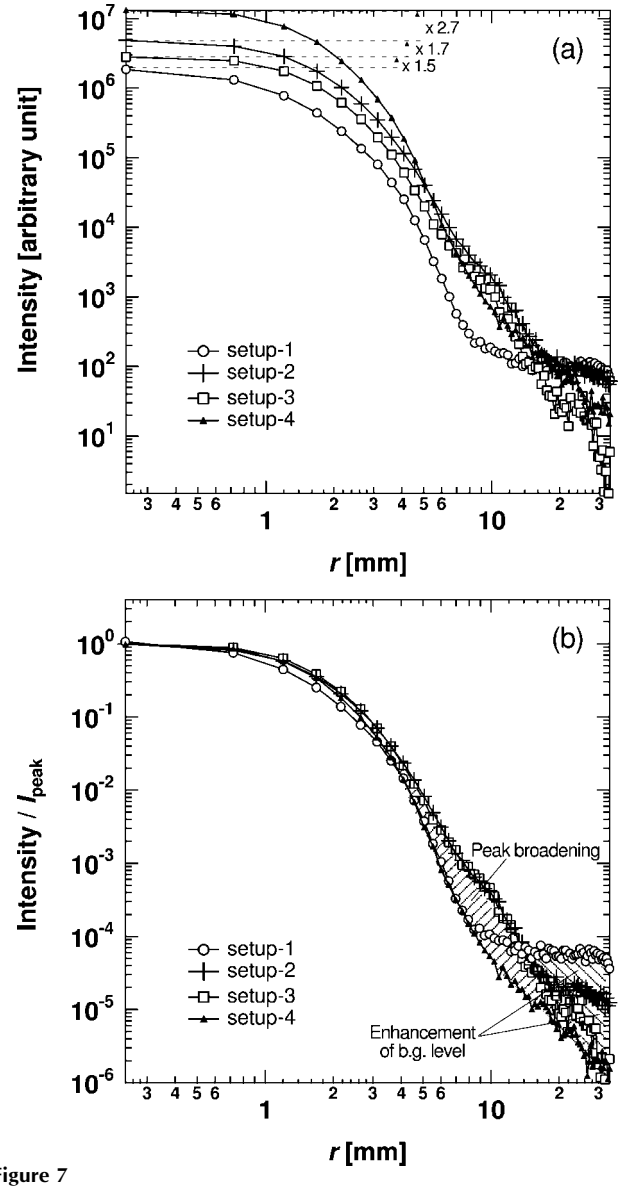

Figure 7
The radial averages of the intensity distribution. (a) The intensities are normalized by the measuring time. (b) The intensities are normalized by the peak intensities $I_{\rm peak}$.

transmission through the 70 MgF_2 lenses was ~0.58 for the setup based on the comparison between setups 2 and 3, and (3) the neutron transmission through the polarizer P2 was ~0.22 for the setup based on the comparison between setups 3 and 4. In terms of the neutron intensity, these results indicate that the magnetic neutron lens is a more efficient neutron focusing device than the compound refractive lenses for SANS experiments using polarized neutrons. Even in experiments in which polarized neutrons are not required, an FSANS experiment could be performed using the magnetic neutron lens as efficiently as in the case of the setup using the compound refractive lenses if a neutron polarizing device with very high neutron transmission is available. Next, we compared the intensity distributions normalized by the peak intensities shown in Fig. 7(b). Peak broadening was observed in setups 2 and 3 with P2 (Fig. 7b). The neutron reflection on the Ni side walls of P2 was considered to be the origin of the peak broadening as illustrated in Fig. 4. The intensity peak profiles of the neutrons focused by the magnetic neutron lens and the compound refractive lenses were found to be very similar except for the background levels (Fig. 7b). Relatively larger enhancement of the background level was observed in setups 1 and 2 with the magnetic neutron lens (Fig. 7b). This can be understood based on the polarity-dependent neutron focusing property of the magnetic neutron lens as follows (Oku *et al.*, 2003): Due to the imperfect neutron polarization, there is a small amount of negative polarity neutrons in the neutron beam coming into the magnetic neutron lens. They are defocused by the magnetic neutron lens and spread over the detector plane, resulting in the enhancement of the background level. The background level of setup 1 was higher than that of setup 2, indicating that the polarizing efficiency of P1 is lower than that of P2.

Here, we estimated the polarization degree of the neutron beam of setups 1 and 2 using the setup of SANS-J-II. Figs. 8(a) and (b) show the intensity distributions of setups 1 and 2, respectively, when the flipper SF is on and off. The peaks that appear with the SF on and off in Figs. 8(a) and (b) are produced by the positive polarity neutrons which are focused by the magnetic neutron lens. Thus, the peak height ratio of $\Delta h_{\mathrm{SF\,on}}/\Delta h_{\mathrm{SF\,off}}$ corresponds to the so-called flipping ratio R. Therefore, we get the relation (Jones & Williams, 1978)

$$R = \frac{\Delta h_{\mathrm{SF\,on}}}{\Delta h_{\mathrm{SF\,off}}} = \frac{1 + P_{\mathrm{i}}P_{\mathrm{a}}(1-D)}{1 + P_{\mathrm{i}}P_{\mathrm{a}}(1-D)(1-2f)}, \qquad (2)$$

where P_{i} and P_{a} are the polarization efficiencies of the polarizer and analyzer, respectively. In this case, the magnetic neutron lens corresponds to the analyzer. f is the flipping efficiency of the SF, D is the depolarization factor. By assuming $P_{\mathrm{a}} = 1$, $f = 1$ and $D = 0$, we obtain

$$P_{\mathrm{i}} = \frac{(\Delta h_{\mathrm{SF\,on}}/\Delta h_{\mathrm{SF\,off}}) - 1}{(\Delta h_{\mathrm{SF\,on}}/\Delta h_{\mathrm{SF\,off}}) + 1}. \qquad (3)$$

From equation (3), we obtained P_i = 0.96 and 0.99 for P1 and P2, respectively. The ratio R_{p} of the peak height P_{h} to the background level B_{l} of the intensity distribution of the direct beam on the detector plane is one of measures which are often used to evaluate SANS instruments. Here, we discuss the relation between R_{p} and the

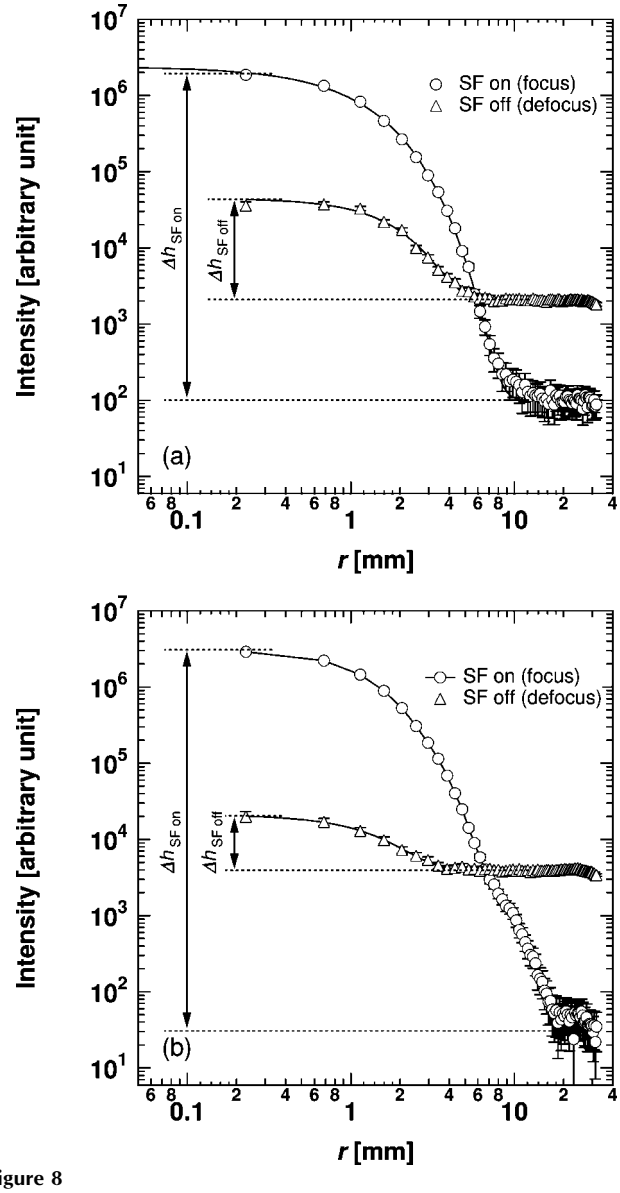

Figure 8
The radial averages of the intensity distribution, when the SF is on and off. (a) For setup 1, (b) for setup 2.

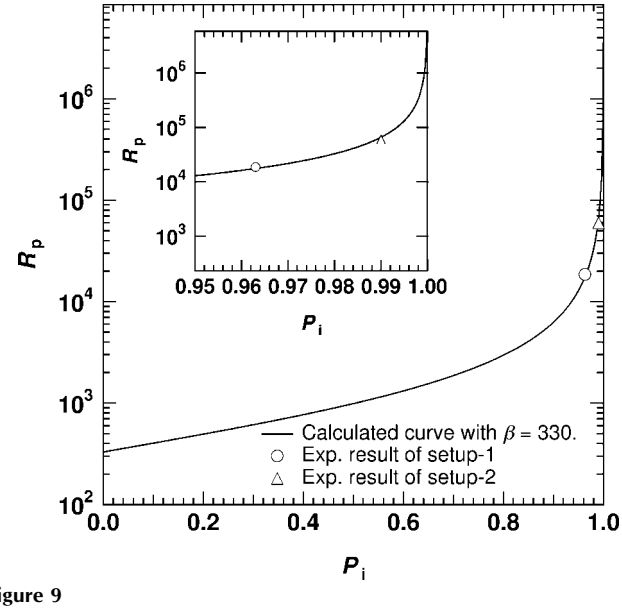

Figure 9
The ratio R_{p} as a function of the polarization efficiency of the polarizer P_{i}. The inset shows an enlargement of the region $0.95 \leq P_{\mathrm{i}} \leq 1$. The open circles and triangles show the experimental values obtained in this study and the solid lines show the calculated values with $\beta = 330$.

polarization degree P of the neutron beam in the FSANS instrument with the magnetic neutron lens. When the magnetic neutron lens is employed as the neutron focusing device, only the positive polarity neutrons are focused by the magnetic neutron lens and create peaks in the intensity distribution on the detector plane. On the other hand, the negative polarity neutrons are defocused by the magnetic neutron lens and homogeneously spread over the detector plane, and raise the background level. Thus, the following relations should hold:

$$P_{\rm h} \propto n_+, \tag{4}$$

$$B_{\rm l} \propto n_-, \tag{5}$$

where n_+ and n_- are the number of positive and negative polarity neutrons going into the magnetic neutron lens, respectively. Based on equations (4) and (5), we get the equation

$$R_{\rm p} = \frac{P_{\rm h}}{B_{\rm l}} = \beta\frac{n_+}{n_-} = \beta R = \beta\frac{1+P_{\rm i}}{1-P_{\rm i}}, \tag{6}$$

where β is a constant that depends on the experimental conditions, and is determined to be $\sim$330 for the current experimental condition based on the experimental results. The calculated values of $R_{\rm p}$ are plotted together with the experimental results as a function of $P_{\rm i}$ in Fig. 9. The inset to Fig. 9 shows the enlargement of the region $0.95 \leq P_{\rm i} \leq 1$. $R_{\rm p}$ increased gradually with increasing $P_{\rm i}$ up to 0.8, followed by a rapid rise with increasing $P_{\rm i}$ up to unity. It is found that a polarizer with $P_{\rm i} \sim 0.999$ is necessary to achieve a value of $R_{\rm p}$ comparable to that of the compound refractive lenses (Fig. 9).

Next, we discuss the key parameters of the q resolution, $\Delta q/q$, and the minimum value of the measurable q range, $q_{\rm min}$, which determine the ability of the SANS instrument [q is the modulus of the scattering vector defined as $q = (4\pi/\lambda)\sin(\theta/2)$ and θ is the scattering angle]. $\Delta q/q$ of the instrument is described by

$$\left(\frac{\Delta q}{q}\right)^2 = \left(\frac{\Delta\lambda}{\lambda}\right)^2 + \left(\frac{\Delta\theta}{\theta}\right)^2. \tag{7}$$

The wavelength dispersion $\Delta\lambda/\lambda$, which is determined by the velocity selector, is 0.13 for the FWHM in this experiment. The angular resolution $\Delta\theta/\theta$ is determined by a convolution of the intensity distribution of the direct beam on the PSD and the position resolution of the PSD. We calculated the $\Delta q/q$ of setups 1 and 2 as a function of q. The results are shown in Fig. 10.

The values of $q_{\rm min}$ were estimated based on the experimental results by using the relation $q_{\rm min} \approx 2\pi r_{\rm min}/(\lambda L_2)$ (Littrell, 2004), where $r_{\rm min}$ was assumed to be the distance from the peak center to where the direct beam intensity becomes 1/1000 of the peak intensity (Fig. 11). To investigate the $\Delta\lambda/\lambda$ dependence of $q_{\rm min}$, we performed numerical simulations under the following conditions: (1) the PSD position resolution and the effect of gravity were taken into account; (2) the experimental values of G = 11 480 T m^{-2} and $P_{\rm i}$ = 0.96 and 0.99 for setups 1 and 2, respectively, were used; (3) an ideal sextupole magnetic field distribution was assumed inside the magnetic neutron lens; and (4) it was assumed that no spin depolarization occurred when the neutrons passed through the magnetic neutron lens. Good agreement was obtained between experimental and simulation values. It is found that about 10 times smaller values of $\Delta q/q$ and $q_{\rm min}$ can be achieved by using the FSANS instrument with the magnetic neutron lens compared with traditional pinhole geometry SANS instruments with an equivalent flight length. According to the simulation results, the resolution can be further increased with increasing $\Delta\lambda/\lambda$ (Fig. 11).

5. Conclusion

We have constructed an FSANS instrument, SANS-J-II, with two kinds of neutron focusing devices: compound refractive lenses made of MgF_2 and a magnetic neutron lens based on an extended Halbach-type sextupole magnet. In this study, we have investigated the performance of the neutron focusing setup using the magnetic neutron lens. The intensity distribution of the direct beam focused on the detector plane by the magnetic neutron lens with a ratio of the peak height to the background level of $\sim 6 \times 10^4$ was obtained using polarized neutrons with a polarization degree of $\sim$ 0.99. The ratio could be further increased by increasing the polarization degree of the neutron beam. $q_{\rm min}$ of 6.5×10^{-4} Å^{-1} could be achieved with $\lambda = 6.6$ Å and $\Delta\lambda/\lambda = 0.13$ for the FWHM. The value of $q_{\rm min}$ can be improved by narrowing the wavelength dispersion.

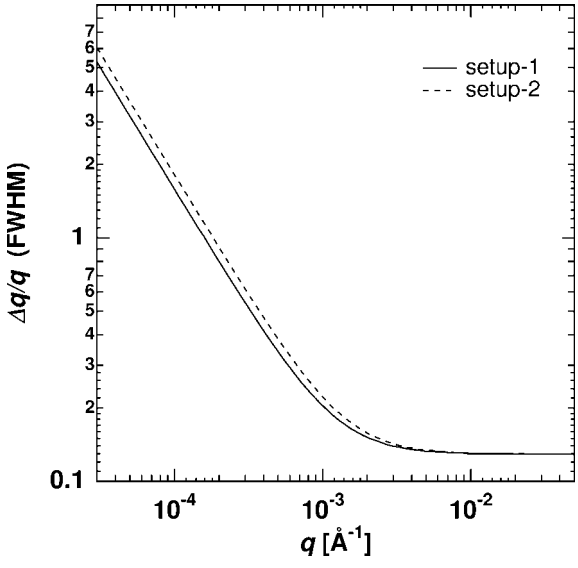

Figure 10
$\Delta q/q$ as a function of q.

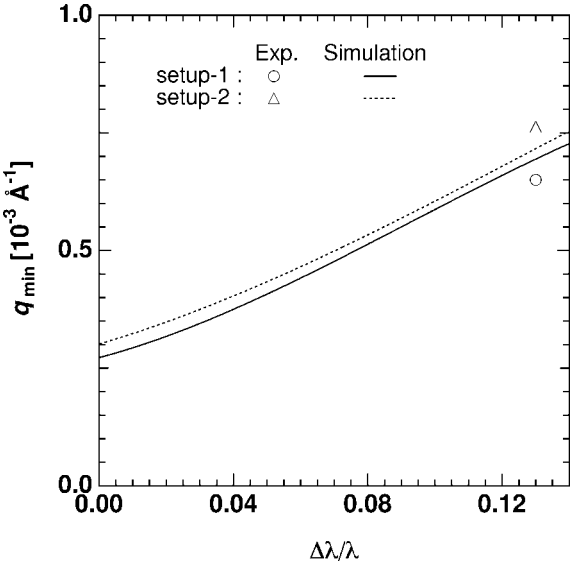

Figure 11
$q_{\rm min}$ *versus* $\Delta\lambda/\lambda$.

This study was partially carried out under the NOP project supported by the Special Coordination Funds for Promoting the Ministry of Education, Culture, Sports, Science and Technology of the Japanese Government.

References

Alefeld, B., Hayes, C., Mezei, F., Richter, D. & Springer,T. (1997). *Physica B*, **234–236**, 1052–1054.

Choi, S.-M., Barker, J. G., Glinka, C. J., Cheng, Y. T. & Gammel, P. L. (2000). *J. Appl. Cryst.* **33**, 793–796.

Eskildsen, M. R., Gammel, P. L., Isaacs, E. D., Detlefs, C., Mortensen, K. & Bishop, D. J. (1998). *Nature (London)*, **391**, 563–566.

Furusaka, M., Niita, K., Suzuki, S., Fujita, K., Suzuki, J., Oku, T., Shimizu, H. M., Otomo, T. & Misawa, M. (1999). *Nucl. Instrum. Methods A*, **529**, 223–230.

Halbach, K. (1979). *IEEE Trans.* **NS-26**, 3882–3884.

Hirota, K., Shinohara, T., Ikeda, K., Mishima, K., Adachi, T., Morishima, T., Satoh, S., Oku, T., Yamada, S., Sasao, H., Suzuki, J. & Shimizu, H. M. (2005). *Phys. Chem. Chem. Phys.* **7**, 1836–1838.

Jones, T. J. L. & Williams W. G. (1978). *Nucl. Instrum. Methods*, **152**, 463–469.

Koizumi, S., Iwase, H., Suzuki, J., Oku, T., Motokawa, R., Sasao, H., Tanaka, H., Yamaguchi, D., Shimizu, H. M. & Hashimoto, T. (2006). *Physica B*, **385–386**, 1000–1006.

Koizumi, S., Iwase, H., Suzuki, J., Oku, T., Motokawa, R., Sasao, H., Tanaka, H., Yamaguchi, D., Shimizu, H. M. & Hashimoto, T. (2007). *J. Appl. Cryst.* **40**, s474–s479.

Kumada, M., Fujisawa, T., Hirao, Y., Endo, M., Aoki, M., Kohda, T., Bolshakova, I. & Holyaka, R. (2001). *Proc. Particle Accelerator Conf.* **5**, 3221–3223.

Littrell, K. C. (2004). *Nucl. Instrum. Methods A*, **529**, 22–27.

Oku, T., Suzuki, J., Adachi, T., Sakai, K., Ikeda, K., Morishima, T., Kiyanagi, Y., Furusaka, M., Tsuzaki, T. & Shimizu, H. M. (2003). *Proc. Int. Collab. Adv. Neutron Sources*, **XVI** 355–362.

Oku, T., Suzuki, J., Sasao, H., Adachi, T., Shinohara, T., Ikeda, K., Morishima, T., Sakai, K., Kiyanagi, Y., Furusaka, M. & Shimizu, H. M. (2004). *Nucl. Instrum. Methods A*, **529**, 116–119.

Oku, T., Suzuki, J., Sasao, H., Yamada, S., Furusaka, M., Adachi, T., Shinohara, T., Ikeda, K. & Shimizu, H. M. (2005). *Physica B*, **356**, 126–130.

Oku, T., Yamada, S., Sasao, H., Suzuki, J., Shinohara, T., Hirota, K., Ikeda, K., Tsuzaki, T., Kiyanagi, Y., Furusaka, M. & Shimizu, H. M. (2006). *Physica B*, **385–386**, 1225–1228.

Shimizu, H. M., Kato, H., Oku, T., Suda, Y., Ogawa, Y., Iwasa, H., Kamiyama, T., Kiyanagi, Y. & Wakabayashi, T. (1998). *Physica B*, **241–243**, 172–174.

Shimizu, H. M., Suda, Y., Oku, T., Nakagawa, H., Kato, H., Kamiyama, T., Otani, C., Sato, H., Wakabayashi, T. & Kiyanagi, Y. (1999). *Nucl. Instrum. Methods A*, **430**, 423–434.

Suzuki, J., Oku, T., Adachi, T., Shimizu, H. M., Hirumachi, T., Tsuchihashi, T. & Watanabe, I. (2003). *J. Appl. Cryst.* **36**, 795–799.